

Fluid Flow in Collapsible Elastic Tubes: A Three-Dimensional Numerical Model

M. E. Rosar and Charles S. Peskin

ABSTRACT. A three-dimensional computer model has been developed to simulate fluid flow through a collapsible tube. The model is based on the immersed boundary method, which is designed to handle a flexible elastic boundary immersed in fluid. This internal boundary is both affected by and has an effect on the motion of the fluid. The setup for collapsible tube simulation involves a fiber-wound elastic tube subjected to an upstream pressure, a downstream pressure, and an external pressure. Partial collapse is observed when the external pressure exceeds the downstream pressure but is less than the upstream pressure. The geometry of the transiently collapsing tube is observed. Collapse is generally localized near the downstream end of the tube, however, under certain conditions, it is also possible for collapse to occur at multiple discrete locations separated by regions of open tubing.

CONTENTS

1. Introduction	281
2. Mathematical formulation	283
3. The tube	286
4. Sources and sinks	288
5. Numerical method	291
6. Simulation results	294
7. Conclusions and future work	300
References	301

1. Introduction

The study of fluid flow through a collapsible elastic tube has multiple applications within the human body. For example Pedley [27] mentions that vessel collapse is

Received March 15, 2001.

Mathematics Subject Classification. 65; 76.

Key words and phrases. collapsible tubes, immersed boundary method, elastic boundary, three-dimensional computation.

This work was supported in part by the National Science Foundation under research grant BIR-9302545. Computation was performed at the Pittsburgh Supercomputing Center under a grant (MCA93S004P) of Cray C-90 computer time from the MetaCenter Allocation Committee.

most readily seen in the veins, such as in the veins of a hand raised above the level of the heart or in the jugular vein when a person is standing erect. Collapse is also observed in the arteries when high external pressures are applied, such as when an artery is compressed by a sphygmomanometer cuff during blood pressure measurement. Kamm and Shapiro [15] also mention the regulation of cardiac output by means of the collapse of the venae cavae as another example of tube collapse in the cardiac system. The pulmonary system also displays collapse, for example, the airways of the lungs can show collapse during coughing or sneezing and during forced or rapid expiration [15, 27]. Self-excited oscillations of collapsible tubes are observed in the laboratory [6, 16], and in certain instances they are also observed *in vivo*, again as when an artery is compressed by a sphygmomanometer cuff [2]. These oscillations may be related to the Korotkoff sounds produced when measuring blood pressure in this way [7, 26].

Flow through a collapsible tube has been extensively studied in the laboratory. The typical experimental setup [6, 15] involves a length of flexible, collapsible tubing mounted at either end on a rigid support. Upstream and downstream fluid reservoirs are provided to drive flow through the tube and to regulate the upstream and downstream pressures. The flexible tube is immersed in air or water in such a manner that the external pressure can be monitored and controlled.

Kamm and Shapiro [15] describe the collapse process, in the presence of an external pressure gradient, as observed in their experiments. They consider the tube collapse as consisting of three phases which they describe as the initial transient phase, the quasi-steady phase, and the viscous drainage phase. The initial transient is identified as a period of flow acceleration giving the initial peak observed in the output flow. The quasi-steady emptying is the period where the output flow drops from its initial peak and where there is “the establishment of a quasi-steady throat in the region of minimum cross-sectional area”. Viscous drainage occurs as the region of collapse increases and the remaining fluid in the tube is forced out as a new equilibrium configuration is approached.

Analytical investigations have typically considered either a lumped-parameter or a one-dimensional model [2, 8, 25, 26]. In a lumped-parameter model the geometry of the collapsing region is represented by one or perhaps several time dependent variables, which are related by ordinary differential equations. In a one-dimensional model, partial differential equations involving only a single spatial coordinate are used. Two-dimensional (channel) models have also been proposed: one of these [20] involves a pair of membranes and another [27] considers a rigid channel with a flexible section in one wall. Analyses have typically derived expressions for the cross sectional area at the point of collapse [19], the fluid flow velocity, and the downstream flow; pressure vs. flow diagrams are studied. The relationship between the shape of the collapsed region and the transmural pressure has also been described [9, 14, 15]. The figure given by Jensen and Pedley in [14] shows how the cross-sectional shape of the tube changes, as the transmural pressure, ($p_{inside} - p_{outside}$), is decreased, going from circular for a fully open tube, becoming elliptical and eventually developing two distinct channels. Such non-axial symmetric collapse supplies a strong motivation for the development of a fully three dimensional approach, which does not rely on any symmetries, to determine the fluid flow and behavior of the tube.

Here we consider such a three dimensional model to determine the motion of the fluid and the tube as a function of time. The model is based upon the immersed boundary method [22, 28, 29, 31, 32, 33]. This method is used to solve the equations of motion of an elastic boundary immersed in a viscous incompressible fluid. These equations are coupled, as the boundary is both affected by and has an effect on the motion of the fluid, and thus the equations of the tube and fluid must be solved simultaneously. The Navier-Stokes equations, governing the fluid dynamics, are solved by a finite difference method. Others have considered alternative methods for immersed boundaries as well [18].

We present a particular tube configuration with a given set of parameters to demonstrate the viability of using the immersed boundary method to address the problem. Exact duplication of laboratory experiments is difficult at this time but detailed studies of collapsible tubes will be addressed in the future.

Although the particular tube that we study exhibits axially symmetric collapse, such symmetry is not imposed a priori. On the contrary, we start the tube in an asymmetric configuration to check the stability of the axially symmetric mode of collapse. We anticipate that changes in tube properties will make axially symmetric collapse unstable, however our method will still be applicable to the asymmetric case, which is the one that is more typically observed in experiments.

Vesier and Yoganathan [39] have also used the immersed boundary method to simulate three-dimensional flow through a flexible elastic tube. The focus of their work was the validation of the method, and they therefore considered a case in which the solution is known through the work of Womersley [40, 41, 42], namely a tube that undergoes small-amplitude, long-wavelength perturbations from its initially cylindrical configuration, these perturbations being driven by a pulsatile flow. In addition, they considered steady flow, simulating Poiseuille flow in a tube. Similarly, we also considered steady flow through a uniform cylindrical tube. Under these conditions, our results agree qualitatively with their results. Velocity profiles in the interior of the tube are parabolic with some deviations at the wall. These deviations were small and can be attributed to the differences between our tube and true Poiseuille flow. Since these results are in agreement with Vesier and Yoganathan, we concur with the validation of the method. We now consider the large-amplitude, short-wavelength deformations that are associated with the phenomenon of partial tube collapse. Partial collapse occurs when the external pressure is greater than the downstream pressure but is less than the upstream pressure. To study the large-amplitude deformations that occur in this situation, we have to introduce a tube model in which computational points are elastically linked to each other, rather than to fixed points in space.

2. Mathematical formulation

We model the flow through a collapsible elastic tube using the immersed boundary method [22, 28, 29, 31, 32, 33]. This involves both a particular way of writing the equations of motion, and also a numerical method for solving those equations. The mathematical formulation will be considered here and the numerical method in a subsequent section. In both cases, the emphasis will be on those aspects that are specific to the current problem of flow in collapsible tubes.

We consider an incompressible, viscous fluid which is treated in an Eulerian manner, with an immersed elastic boundary which is treated in a Lagrangian manner. The boundary, which is modeled as a collection of massless fibers, applies a force to the fluid in which it is immersed and is moved by the fluid at the local fluid velocity. The force of the boundary on the fluid is determined by the boundary configuration and by the assumed elastic properties of the boundary.

Note in particular that we postulate the same fluid inside and outside the tube, and that the mass in the problem is provided by the fluid (both inside and out) and not by the tube per se. While these assumptions might be a limitation for some applications such as airflow in the lung, they are right on target for the problem of blood flow. This is because the tissue outside a typical blood vessel has about the same density as blood. (There are exceptions to this, of course, such as a blood vessel in a bone, or a blood vessel in the lung, or a blood vessel close to the skin.) The inertial and viscous loads provided by the external tissue are presumably important and are included in our model. They would be neglected by treating the external medium as a constant-pressure boundary condition, as is commonly done. One could go further in our direction and model the elastic properties of the external tissue as well. This could be done within our framework by laying down elastic fibers in the space external to the tube, instead of just on the tube wall, as we have done here.

The motion of the fluid is governed by the incompressible Navier-Stokes equations:

$$(1) \quad \rho \left(\frac{\partial \mathbf{u}(\mathbf{x}, t)}{\partial t} + \mathbf{u}(\mathbf{x}, t) \cdot \nabla \mathbf{u}(\mathbf{x}, t) \right) + \nabla p(\mathbf{x}, t) = \mu \Delta \mathbf{u}(\mathbf{x}, t) + \mathbf{F}(\mathbf{x}, t)$$

$$(2) \quad \nabla \cdot \mathbf{u}(\mathbf{x}, t) = 0,$$

with $\mathbf{x} = (x_1, x_2, x_3)$. $\mathbf{F}(\mathbf{x}, t)$ is the force density resulting from the fibers of the immersed boundary. These forces will be specified below. Since we consider the case of a massless tube with the same fluid inside and out, the effect of gravity can be absorbed into a redefinition of the pressure, after which gravity no longer appears in the equations. We assume here that this has already been done. Thus, in the above equations, $p(\mathbf{x}, t)$ is the deviation of the pressure from the hydrostatic pressure at level x_3 . The particular collapsible tube model we are considering functions in exactly the same way in orbit as on Earth.

The Navier-Stokes equations are given in Cartesian coordinates, with $\mathbf{x} = (x_1, x_2, x_3)$. The fibers, which give the boundary its elasticity, however, are described in curvilinear coordinates (q, s) , where $q = \text{constant}$ is the equation of a fiber, s locates the position along a fiber, and (q, s) are both constant for any material point. Note that s may be the arclength in some particular initial configuration, but it is not the arclength in general since the fibers change length as the tube is deformed; the distance along a fiber between any two material points need not remain constant.

The above description applies to a thin-walled tube in which the wall has been idealized as a surface. Note, however, that it is straightforward to model a thick-walled tube by introducing an additional parameter r that locates a layer of fibers within the thickness of the wall. In that case, since the fibers themselves are massless but are immersed in the same incompressible fluid that is found inside

and outside the tube, the simulated thick wall acts as an incompressible, fiber-reinforced, neutrally buoyant, elastic material. In this paper, however, we confine ourselves to the thin-walled case.

The positions, \mathbf{X} , of the points of the fibers may be given in terms of these curvilinear coordinates by $\mathbf{X}(q, s, t)$ at the time t . In terms of these curvilinear coordinates, the motion of the boundary is described as $\mathbf{x} = \mathbf{X}(q, s, t)$. Our goal is to determine the function $\mathbf{X}(q, s, t)$ along with the motion of the fluid $\mathbf{u}(\mathbf{x}, t)$.

Because of the fiber elasticity, there is a mapping from the fiber point positions \mathbf{X} to the density of the force supplied by the fibers, given by

$$(3) \quad \mathbf{X}(\cdot, \cdot, t) \longrightarrow \mathbf{f}(\cdot, \cdot, t).$$

We thus write the force as a function dependent on the positions \mathbf{X} of the fiber points,

$$(4) \quad \mathbf{f}(\cdot, \cdot, t) = \mathcal{S}[\mathbf{X}(\cdot, \cdot, t)].$$

The exact nature of this dependence is determined by the elastic properties of the fibers and will be considered in more detail later.

These forces are calculated at the fiber coordinates and are then transferred to the fluid. But since the fluid equations are written in Cartesian coordinates, we need the total force density in Cartesian coordinates, such that

$$(5) \quad \int_{\mathcal{D}} \mathbf{F}(\mathbf{x}, t) \, d\mathbf{x} = \int_{\mathbf{X}(q, s, t) \in \mathcal{D}} \mathbf{f}(q, s, t) \, dq \, ds$$

where \mathcal{D} is some arbitrary domain in (x, y, z) -space. $\mathbf{F}(\mathbf{x}, t)$ can be defined explicitly by means of the three dimensional Dirac δ function,

$$(6) \quad \mathbf{F}(\mathbf{x}, t) = \int \mathbf{f}(q, s, t) \delta(\mathbf{x} - \mathbf{X}(q, s, t)) \, dq \, ds,$$

where the integral is taken over all the fiber points. Note that this is an integration over only two spatial dimensions although the δ function in the integrand is three dimensional. This defines $\mathbf{F}(\mathbf{x}, t)$ as a distribution with support on the fiber surface. The function $\mathbf{F}(\mathbf{x}, t)$ is singular like a one dimensional δ function, and thus is infinite on the boundary, while the integral of $\mathbf{F}(\mathbf{x}, t)$ over any finite volume remains finite. To check that the explicit formula for $\mathbf{F}(\mathbf{x}, t)$ satisfies the implicit condition that precedes it, integrate over the arbitrary domain \mathcal{D} , interchange the order of integration, and use the properties of the Dirac δ function.

As noted above, the fiber points will move at the local fluid velocity, which is the no-slip condition for a viscous fluid. Thus, given a fluid velocity field $\mathbf{u}(\mathbf{x}, t)$, the local fluid velocity must also be determined in terms of the fiber coordinates. This is again done by using the Dirac δ function,

$$(7) \quad \mathbf{U}(q, s, t) = \int \mathbf{u}(\mathbf{x}, t) \delta(\mathbf{x} - \mathbf{X}(q, s, t)) \, d\mathbf{x}.$$

To drive the fluid through the tube, and to regulate the transmural pressure difference, we allow for sources and sinks, each having a spatial strength distribution, $\psi(\mathbf{x})$, and a volume flow rate $Q(t)$. Their presence makes a contribution to the continuity equation. Combining all these, we have the complete system of equations, which we write down here:

$$(8) \quad \rho \left(\frac{\partial \mathbf{u}}{\partial t} + \mathbf{u} \cdot \nabla \mathbf{u} \right) + \nabla p = \mu \Delta \mathbf{u} + \mathbf{F}$$

$$(9) \quad \nabla \cdot \mathbf{u}(\mathbf{x}, t) = \sum_{j=0}^m Q_j(t) \psi_j(\mathbf{x})$$

$$(10) \quad \mathbf{F}(\mathbf{x}, t) = \int \mathbf{f}(q, s, t) \delta(\mathbf{x} - \mathbf{X}(q, s, t)) dq ds$$

$$(11) \quad \frac{\partial \mathbf{X}}{\partial t}(q, s, t) = \mathbf{U}(q, s, t) = \int \mathbf{u}(\mathbf{x}, t) \delta(\mathbf{x} - \mathbf{X}(q, s, t)) d\mathbf{x}$$

$$(12) \quad \mathbf{f}(\cdot, \cdot, t) = \mathcal{S}[\mathbf{X}(\cdot, \cdot, t)].$$

The first two equations are the Navier-Stokes equations for the fluid including sources and sinks. The last equation is the equation of the boundary. The remaining two equations give the interaction between the fluid and the boundary.

3. The tube

The boundary we choose in the present application of the immersed boundary method is an elastic cylindrical tube through which the fluid will flow. It is composed of fibers of points, where we use the term fiber in a general sense to mean a collection of sequentially connected points. Although we speak of all the points as being on fibers, not all of the fibers behave in the same way, and thus we must make a distinction among them. In developing this tube model we look to applications, in particular that of blood flow in veins. We use the structure of veins as a guide in the selection of the types of fibers which are used. It is well known that elastic fibers in vein walls may run longitudinally, transversely, or obliquely. Bundles of collagenous and elastic fibers as well as smooth muscle cells form helices in the vein wall, winding in opposite directions. This arrangement adds to the strength and support of the vein walls [36]. We use this structure in our model. Thus, our tube is composed of two sets of helical fibers, winding about the tube in opposite senses, a set of straight beam-like stiffening fibers running the length of the tube without winding around the tube, and a collection of rings or hoops, equally spaced along the length of the tube. The ends of the fibers, as well as the first and last ring, will remain approximately fixed in space. The rest of the tube will be free to move at the local fluid velocity and will apply forces locally to the fluid.

By using fibers (in the above generalized sense) as the elements from which we construct our tube, we admittedly make it difficult to model the kinds of tubes that are often used in experiments, which are essentially shells made of homogeneous isotropic material. Biological tissue, however, is rarely isotropic and has a fibrous organization involving several different kinds of fibers: collagen, elastin, etc. On the other hand, we freely admit that the particular arrangement of fibers used here is only preliminary, and that more work is needed to construct a realistic fiber-based model of a blood vessel wall. Such a model would, for example, have multiple layers of helical fibers with different helical pitches, rather than the single pair of mirror-image helical layers used here. It will be interesting to study the effect of the fiber architecture on the manner in which the vessel collapses, but that remains for future work.

As noted previously, we define curvilinear coordinates for the fibers, (q, s, t) , where q designates a fiber, $s =$ arclength along the fiber (at time 0), and $t =$ time. Note that the coordinate s is the arclength from the “beginning” of the fiber at the time $t = 0$, i.e., the initial distance along the fiber from the starting point of the fiber. Note also that this starting point is somewhat arbitrary. We choose these initial points for convenience. So for the helices and straight fibers the initial position is chosen to be one end of the cylinder. We will use $q = \theta$ to identify the fiber by its initial angular location on the circle at the upstream end of the cylinder. In addition to the two sets of helical fibers winding their way around and along the tube, we also include a set of straight fibers and hoops, or rings, positioned along the length of the collapsible tube. In laboratory experiments, the flexible tubing is typically mounted on rigid support tubes located at each end of the collapsible tube. These are simulated by a series of rings of points, located between the ends of the collapsible tube and the “caps,” which are defined next. Each end of the tube has a cap closing off the tube, composed of a section of a sphere. The caps are made up of points arranged in rings which form “latitude lines” of the sphere, and a point at the pole. A fluid flow source is located at the center of the sphere comprising the cap at the upstream end; similarly a sink is located at the center of the spherical cap at the downstream end. The source and sink are meant to simulate an input reservoir and outflow reservoir. Their properties are described below.

With the tube geometry defined we can determine the forces generated by the fibers which will, in turn, act on the fluid. The forces are given by the gradient of the elastic energy in the fibers. The energy may be written as [22, 30, 31]

$$\begin{aligned}
 (13) \quad E = & \frac{1}{2} S_{0,H_r} \int_0^{2\pi} \int_0^{L_H} \left(\left| \frac{\partial \mathbf{X}_{H_r}}{\partial s} \right| - 1 \right)^2 ds d\theta \\
 & + \frac{1}{2} S_{0,H_l} \int_0^{2\pi} \int_0^{L_H} \left(\left| \frac{\partial \mathbf{X}_{H_l}}{\partial s} \right| - 1 \right)^2 ds d\theta \\
 & + \frac{1}{2} S_{0,B} \int_0^{2\pi} \int_0^L \left| \frac{\partial^2 \mathbf{X}_B}{\partial s^2} \right|^2 ds d\theta \\
 & + \frac{1}{2} S_{0,R_s} \int_0^L \int_0^{2\pi r} \left(\left| \frac{\partial \mathbf{X}_R}{\partial s} \right| - 1 \right)^2 ds dx \\
 & + \frac{1}{2} S_{0,R_b} \int_0^L \int_0^{2\pi r} \left| \frac{\partial^2 \mathbf{X}_R}{\partial s^2} \right|^2 ds dx
 \end{aligned}$$

where we have written the energy as a sum of five terms, each being the contribution due to a different set of fibers. L_H is the total, unstressed length of a helical fiber, L is the unstressed length of a straight beam-like fiber (length of the collapsible tube), and r is the unstressed radius of the rings (radius of the fully open tube). S_{0,H_r} and S_{0,H_l} are stiffness constants for the two (right-handed and left-handed) sets of helical fibers; $S_{0,B}$ is a stiffness constant for the “beam” fibers; and S_{0,R_s} and S_{0,R_b} are spring-like and beam-like stiffness constants for the ring fibers. Note that we have indexed the point positions on the various sets of fibers differently, for, even though both sets of helices, the straight fibers and the rings define the same cylinder, they parameterize it differently.

The first two terms are the contributions due to the helical fibers. The expression $(|\frac{\partial \mathbf{X}}{\partial s}| - 1)$ gives a measure of the deviation of the separation of consecutive points on a fiber from a given unstressed point separation, relative to that unstressed separation. These fibers will thus resist stretching and compression. The third term is the contribution due to the straight beam-like fibers. This term is determined by the second derivative of the point positions with respect to arclength and thus will give a bending rigidity to the beams. The last two terms represent the contribution of the hoops to the elastic energy of the tube. One term has a contribution like that of the helical fibers and the other a contribution like that of the beams. Thus the hoops will have both stretching and compression rigidity as well as bending rigidity. During steady flow, the fibers are stretched by about 1% relative to their unstretched configuration.

The above formula for the elastic energy is discretized by using finite difference formulae for the derivatives and summations for the integrals. Let E_l be the contribution of the l -th discrete fiber to the total elastic energy. Note that E_l is the discrete elastic energy of the discrete fiber l , not the energy density evaluated on that fiber. The force at the (l, m) -th boundary point, i.e., the m -th point on the l -th fiber (which may be a helical fiber, a beam, or a hoop), is given by

$$(14) \quad \mathbf{f}(l, m) = -\nabla_{l,m} E_l = -\left(\frac{\partial E_l}{\partial x_1(l, m)} \mathbf{i} + \frac{\partial E_l}{\partial x_2(l, m)} \mathbf{j} + \frac{\partial E_l}{\partial x_3(l, m)} \mathbf{k} \right)$$

where we used the subscript l, m on ∇ to denote the m -th point on the l -th fiber. Note that $f(l, m)$, as defined by this formula is the discrete force, not force density, applied to the fluid by the m -th point of the l -th fiber.

It was noted above that the collapsible tube is mounted on rigid supports at each end. These are given by a sequence of points arranged in rings, located between the ends of the tube and the end caps. The length of these extensions is twice the radius of the tube, but the length may be varied. Indeed, different lengths were tried, showing no significant variation in the results due to varying extension length.

The force at any of the points of the rigid extensions and tube caps which hold the upstream source and downstream sink is a Hooke's law restoring force, relative to fixed points in space, namely the initial position of the point as defined in the construction phase. They provide a feedback mechanism which tends to keep these points approximately fixed at their initial locations. Although we sometimes speak of these points as "fixed", or the structures that they comprise as "rigid", it should be noted that they have to move slightly in order to develop the forces that here simulate the zero-velocity boundary condition that is normally applied along a fixed, rigid boundary.

Finally all the terms that contribute force at a given fiber point are added. This yields the total force that must be applied to the fluid in the neighborhood of that fiber point.

4. Sources and sinks

The simulated tube is provided with an external source/sink, an upstream source, and a downstream sink, the spatial distributions of which are defined by specifying

three non-negative functions $\psi_j(\mathbf{x}), j = 0, 1, 2$, respectively, such that

$$(15) \quad \int \psi_j(\mathbf{x}) d\mathbf{x} = 1.$$

That the integral of ψ_j is equal to 1 has dual significance. First, in the formula for the divergence of \mathbf{u} that is given below, it ensures that $Q_j(t)$ can be interpreted as the total flux through source j at time t . Second, it will allow the same function ψ_j to be used as a weight function in defining the average pressure at the location of the source or sink described by ψ_j .

The support of ψ_0 is taken to be a thin planar slab parallel to the axis of the tube but external to the tube. The external source/sink described by ψ_0 is needed to allow changes in volume of the tube, and also to provide a reference pressure relative to which the other source and sink pressures can be defined. ψ_1 and ψ_2 are treated as small spherical sources (which may be seen as point sources spread over several grid points in each direction). The support of ψ_1 is localized within the sphere that defines the upstream cap, and the support of ψ_2 is localized within the sphere that defines the downstream cap.

The volume rate of flow at source or sink j will be denoted $Q_j(t)$, positive for a source and negative for a sink. The manner in which the Q_j are specified will be described below. The sources and sinks appear in the fluid equations through the continuity equation

$$(16) \quad \nabla \cdot \mathbf{u}(\mathbf{x}, t) = \sum_{j=0}^2 Q_j(t) \psi_j(\mathbf{x}).$$

Since our domain will be taken to be periodic (see below),

$$(17) \quad \int \nabla \cdot \mathbf{u}(\mathbf{x}, t) d\mathbf{x} = \mathbf{0}.$$

Therefore, we must impose the restriction

$$(18) \quad \sum_{j=0}^2 Q_j(t) = 0.$$

We use this to determine Q_0 once Q_1 and Q_2 are known.

In the numerical experiments reported here, the upstream flow Q_1 is held constant, and the downstream flow Q_2 is chosen to simulate the situation in which the downstream sink is connected to a pressure reservoir through a nonlinear hydraulic resistance (with inertia), the specific form of which is specified below. This downstream condition was chosen because it simulates the downstream conditions imposed in the classic collapsible-tube experiments of Conrad [6].

To specify the relationship between flow and pressure at the downstream sink, we first need to define the pressure at that location. This is done as follows. Let

$$(19) \quad P_2(t) = \int p(\mathbf{x}, t) \psi_2(\mathbf{x}) d\mathbf{x}$$

where $p(\mathbf{x}, t)$ is the pressure field of the fluid. To make this pressure meaningful, however, we need to compare it to some reference pressure. A convenient reference

is the pressure at the external source/sink:

$$(20) \quad P_0(t) = \int p(\mathbf{x}, t) \psi_0(\mathbf{x}) d\mathbf{x}.$$

Thus, the pressure at the downstream sink is taken to be

$$(21) \quad \tilde{P}_2(t) = P_2(t) - P_0(t).$$

Note that $\tilde{P}_2(t)$ remains invariant if we add an arbitrary constant, or even an arbitrary function of time, to the pressure field $p(\mathbf{x}, t)$.

Now that the pressure $\tilde{P}_2(t)$ at the downstream sink is defined, we can specify how the flow $Q_2(t)$ is related to that pressure. The relationship that we impose is the following:

$$(22) \quad \tilde{P}_2^* - \tilde{P}_2(t) = R_2 Q_2 + K_2 |Q_2| Q_2 + L_2 \frac{dQ_2}{dt},$$

where \tilde{P}_2^* , R_2 , K_2 , and L_2 are given constants. The constant \tilde{P}_2^* represents the pressure in a reservoir to which the downstream sink is connected. The pressure drop across the connection between the sink and the reservoir is assumed to have three components: a linear hydraulic resistance characterized by the coefficient R_2 , a square-law hydraulic resistance characterized by the coefficient K_2 , and an inertance characterized by the coefficient L_2 . Note that the pressure drop across the square-law resistance involves $|Q_2|Q_2$ rather than Q_2^2 , since the pressure should always decrease across this nonlinear component when it is traversed in the direction of the flow. The two types of hydraulic resistance are included because they are typically present downstream in experiments on collapsible tubes [6]. The inertance is included primarily to avoid a numerical instability (see below), although it is certainly not wrong to include an inertance, since real fluids inevitably have inertia.

The numerical scheme that we use to determine Q_2^{n+1} , the value of Q_2 at the $n + 1$ time step, is as follows:

$$(23) \quad \tilde{P}_2^* - \tilde{P}_2^n = R_2 Q_2^{n+1} + K_2 |Q_2^{n+1}| Q_2^{n+1} + L_2 \frac{Q_2^{n+1} - Q_2^n}{\Delta t}.$$

This is the backward-Euler method, except that we use \tilde{P}_2^n instead of \tilde{P}_2^{n+1} . This choice is made for convenience even though it does adversely affect the stability of the scheme. Indeed, to maintain stability, it was necessary to decrease the time step by a factor of four, compared to that required by the velocity solver. (Note that we are not dealing merely with the above ordinary differential equation for Q_2 ; that equation is coupled through the pressure to the Navier-Stokes equations for the fluid.) The alternative of using \tilde{P}_2^{n+1} , which is coupled to Q_2^{n+1} through the fluid mechanics, is indeed feasible [29], but it is complicated and somewhat computationally expensive. We opt here for the simpler alternative of using \tilde{P}_2^n . It is this choice, however, that makes it necessary to introduce at least a small inertance (suggested by David McQueen [21]) to stabilize the sink flow. Without that inertance we observed a peculiar numerical instability that gets worse as the time step is reduced.

Despite the nonlinearity, it is clear that the above equation for Q_2^{n+1} has exactly one solution, since the right-hand side is an unbounded monotonic function of Q_2^{n+1} . The solution can be found by noting that the equation for Q_2^{n+1} is a quadratic

equation for $Q_2^{n+1} > 0$ and a different quadratic equation for $Q_2^{n+1} < 0$. These two quadratic equations together have at most four roots. Each root can be tested for self-consistency. If it is a root of the quadratic equation that was derived by assuming $Q_2^{n+1} > 0$, then it is a solution to our problem if and only if it is indeed greater than zero. Similarly, if it is a root of the quadratic equation that was derived by assuming $Q_2^{n+1} < 0$, then it is a solution to our problem if and only if it is indeed less than zero. But we have just proved that our problem has exactly one solution, so it must be the case that one and only one of four roots of the two quadratic equations will pass this consistency test. That is the one we actually use.

5. Numerical method

The numerical method used in this work is an immersed boundary method [22, 28, 29, 31, 32, 33]. The fluid equations are discretized on a regular cubic lattice with periodic boundary conditions, the structure of which is not disturbed in any way by the immersed elastic boundary. Communication in both directions between the immersed boundary and the fluid is accomplished by using an approximation δ_h to the Dirac delta function. The specific choice of δ_h used in this work is

$$(24) \quad \delta_h(x) = \begin{cases} \frac{1}{4h} (1 + \cos \frac{\pi x}{2h}), & |x| \leq 2h \\ 0, & |x| \geq 2h. \end{cases}$$

From this, the three-dimensional δ_h is defined by

$$(25) \quad \delta_h(\mathbf{x}) = \delta_h(x_1)\delta_h(x_2)\delta_h(x_3)$$

where $\mathbf{x} = (x_1, x_2, x_3)$. The motivation for this choice of δ_h is discussed in [29].

The Navier-Stokes solver used is an implementation of the projection method [4, 5]. A non-standard feature, however, is our choice of the divergence and gradient operators, which are “tuned” to the choice of δ_h in a way that will be described below. This makes a dramatic improvement in the volume-conservation properties of the immersed boundary method [35, 37, 38].

The spatial difference operators used in this work will now be defined. First, we introduce the standard forward, backward, and central difference operators in the three space directions:

$$(26) \quad (D_s^+ \phi)(\mathbf{x}) = \frac{\phi(\mathbf{x} + h\mathbf{e}_s) - \phi(\mathbf{x})}{h}$$

$$(27) \quad (D_s^- \phi)(\mathbf{x}) = \frac{\phi(\mathbf{x}) - \phi(\mathbf{x} - h\mathbf{e}_s)}{h}$$

$$(28) \quad (D_s^0 \phi)(\mathbf{x}) = \frac{\phi(\mathbf{x} + h\mathbf{e}_s) - \phi(\mathbf{x} - h\mathbf{e}_s)}{2h}$$

where $s = 1, 2, 3$ and \mathbf{e}_s represents the unit vector in the s direction. These operators are used in the viscous and convection terms of the Navier-Stokes equations:

$$(29) \quad \Delta \mathbf{u} \approx \sum_{s=1}^3 D_s^+ D_s^- \mathbf{u}$$

$$(30) \quad \mathbf{u} \cdot \nabla \mathbf{u} \approx \sum_{s=1}^3 u_s D_s^0 \mathbf{u}.$$

As mentioned above, the divergence and gradient operators, which appear in the projection step of the projection method, are not defined from the standard difference operators but rather according to a recipe that takes the function δ_h into account. Let \mathbf{x} denote a grid point and \mathbf{X} an arbitrary point in space. The interpolated velocity field in which the immersed boundary moves is defined by

$$(31) \quad \mathbf{U}(\mathbf{X}) = \sum_{\mathbf{x}} \mathbf{u}(\mathbf{x}) \delta_h(\mathbf{x} - \mathbf{X}) h^3$$

where $\sum_{\mathbf{x}}$ denotes the sum over the cubic lattice of the fluid. By the properties of δ_h , $\mathbf{U}(\mathbf{X})$ is continuous with continuous first derivatives. Then, since $\nabla \cdot \mathbf{U}$ is well defined, we may define the operator \mathbf{D} such that

$$(32) \quad (\mathbf{D} \cdot \mathbf{u})(\mathbf{x}) = h^{-3} \int_{B(\mathbf{x})} (\nabla \cdot \mathbf{U})(\mathbf{X}) d\mathbf{X}$$

where $B(\mathbf{x})$ is a cube of side h with edges aligned with the grid and centered on the grid point \mathbf{x} . Note that $(\mathbf{D} \cdot \mathbf{u})(\mathbf{x})$ is the average of $\nabla \cdot \mathbf{U}$ over the cube $B(\mathbf{x})$. After applying the divergence theorem to the above equation, substituting the above expression for $\mathbf{U}(\mathbf{X})$, and using the fact that δ_h is an even function, we may write the discrete divergence \mathbf{D} of $\mathbf{u}(\mathbf{x})$, in three dimensions, as

$$(33) \quad (\mathbf{D} \cdot \mathbf{u})(\mathbf{x}) = \sum_{\mathbf{x}'} [u_1(x'_1, x'_2, x'_3) \gamma(x_1 - x'_1) \omega(x_2 - x'_2) \omega(x_3 - x'_3) \\ + u_2(x'_1, x'_2, x'_3) \omega(x_1 - x'_1) \gamma(x_2 - x'_2) \omega(x_3 - x'_3) \\ + u_3(x'_1, x'_2, x'_3) \omega(x_1 - x'_1) \omega(x_2 - x'_2) \gamma(x_3 - x'_3)]$$

where $\mathbf{x} = (x_1, x_2, x_3)$ and $\mathbf{x}' = (x'_1, x'_2, x'_3)$, and with

$$(34) \quad \gamma(x) = \delta_h(x + X) \Big|_{X=-h/2}^{X=h/2}$$

$$(35) \quad \omega(x) = \int_{-h/2}^{h/2} \delta_h(x + X) dX.$$

As the notation $\mathbf{D} \cdot \mathbf{u}$ suggests, the foregoing definition of \mathbf{D} is indeed of the form

$$(36) \quad \mathbf{D} \cdot \mathbf{u} = D_1 u_1 + D_2 u_2 + D_3 u_3,$$

where the operators D_1 , D_2 , and D_3 are defined as follows:

$$(37) \quad (D_1 \phi)(x_1, x_2, x_3) = \sum_{(x'_1, x'_2, x'_3)} \phi(x_1, x_2, x_3) \gamma(x_1 - x'_1) \omega(x_2 - x'_2) \omega(x_3 - x'_3)$$

$$(38) \quad (D_2 \phi)(x_1, x_2, x_3) = \sum_{(x'_1, x'_2, x'_3)} \phi(x_1, x_2, x_3) \omega(x_1 - x'_1) \gamma(x_2 - x'_2) \omega(x_3 - x'_3)$$

$$(39) \quad (D_3 \phi)(x_1, x_2, x_3) = \sum_{(x'_1, x'_2, x'_3)} \phi(x_1, x_2, x_3) \omega(x_1 - x'_1) \omega(x_2 - x'_2) \gamma(x_3 - x'_3).$$

We can use these operators not only for the discrete divergence but also for the discrete gradient. Thus

$$(40) \quad \mathbf{D}\phi(\mathbf{x}) = ((D_1 \phi)(\mathbf{x}), (D_2 \phi)(\mathbf{x}), (D_3 \phi)(\mathbf{x}))$$

is the expression that we shall use for the gradient of ϕ .

At the beginning of the n th time step, the fluid velocity \mathbf{u}^n and the boundary configuration \mathbf{X}^n are known. The pressure p^n is also known, since it was computed

along with \mathbf{u}^n during the projection step at the previous time step. The pressure field can be used to update the source and sink flows in the manner described above. Once this has been done Q_j^{n+1} is known, for $j=0,1,2$. Our task now is to update the velocity and pressure fields, and also the immersed boundary configuration. This is done as follows.

First compute \mathbf{f}^n from the boundary configuration \mathbf{X}^n . The details of how to do this have been described above, in Section 3. Next, use the function δ_h to apply this force to the fluid:

$$(41) \quad \mathbf{F}^n(\mathbf{x}) = \sum_{l,m} \mathbf{f}(l, m) \delta_h(\mathbf{x} - \mathbf{X}(l, m)).$$

Once \mathbf{F} has been defined on the fluid lattice, we can use the projection method [4, 5] to integrate the Navier-Stokes equations. The steps are as follows: First, let

$$(42) \quad \mathbf{u}^{n,0} = \mathbf{u}^n + \frac{\Delta t}{\rho} \mathbf{F}^n.$$

Next, solve successively the following systems of equations for $\mathbf{u}^{n,1}$, $\mathbf{u}^{n,2}$, and $\mathbf{u}^{n,3}$:

$$(43) \quad \rho \left[\frac{(\mathbf{u}^{n,1} - \mathbf{u}^{n,0})}{\Delta t} + u_1^n D_1^0 \mathbf{u}^{n,1} \right] = \mu D_1^+ D_1^- \mathbf{u}^{n,1}$$

$$(44) \quad \rho \left[\frac{(\mathbf{u}^{n,2} - \mathbf{u}^{n,1})}{\Delta t} + u_2^n D_2^0 \mathbf{u}^{n,2} \right] = \mu D_2^+ D_2^- \mathbf{u}^{n,2}$$

$$(45) \quad \rho \left[\frac{(\mathbf{u}^{n,3} - \mathbf{u}^{n,2})}{\Delta t} + u_3^n D_3^0 \mathbf{u}^{n,3} \right] = \mu D_3^+ D_3^- \mathbf{u}^{n,3}.$$

Note that each of these involves coupling in one spatial direction only, and thus constitutes a collection of periodic tridiagonal systems [34].

The final step in integrating the Navier-Stokes equations is the projection step, in which we solve the following system for \mathbf{u}^{n+1} and p^{n+1} :

$$(46) \quad \rho \left(\frac{\mathbf{u}^{n+1} - \mathbf{u}^{n,3}}{\Delta t} \right) + \mathbf{D} p^{n+1} = 0$$

$$(47) \quad \mathbf{D} \cdot \mathbf{u}^{n+1} = \sum_{j=0}^2 Q_j(t) \psi_j.$$

The equations of the projection step are linear with constant coefficients, and the fluid domain is a periodic box. Thus, the projection step can be carried out with the help of the Fast Fourier Transform. The implementation of this idea is complicated by the rather intricate construction of the operator \mathbf{D} , (see above), but this does not impair the efficiency of the scheme, since the Fourier transform of this operator can be precomputed and stored. For details, see [37, 38].

Once the fluid velocity is known at the grid points, the positions of the boundary points can be updated as follows:

$$(48) \quad \mathbf{X}^{n+1}(l, m) = \mathbf{X}^n(l, m) + \Delta t \sum_{\mathbf{x}} \mathbf{u}^{n+1}(\mathbf{x}) \delta_h(\mathbf{x} - \mathbf{X}^n(l, m)) h^3,$$

in which, as before, $\sum_{\mathbf{x}}$ denotes the sum over the computational lattice of the fluid. Thus the positions of the boundary points are updated by moving the boundary points at the local (interpolated) fluid velocity. This completes the time step and

the process is repeated by calculating the new force imposed by the new boundary configuration, etc.

6. Simulation results

The situation we simulate is that of a long, thin-walled, collapsible tube mounted on rigid cylindrical supports. As discussed above, the wall of the tube is comprised of fibers of several different types: helical fibers that resist changes in length from a prescribed rest length, longitudinal fibers that resist bending and also supply longitudinal tension, and fiber rings that resist length changes and bending. We report here one particular instance of the tube and parameters to demonstrate the efficacy of the three-dimensional computational model. Detailed comparative analyses of collapsible tubes will be presented in future reports. The lattice used to simulate the experiment is taken to be 20 cm x 2.5 cm x 2.5 cm, with 256 x 32 x 32 points and a lattice spacing of $h = \frac{20}{256} (= 0.078125)$ cm in each direction. The collapsible tube is 10 cm in length with a radius of 0.625 cm. Each rigid extension has a length equal to twice the radius of the tube. The upstream flow rate is set to $Q_1 = 15\text{cm}^3/\text{sec}$. The downstream reservoir pressure is set to -29.4 mm Hg $\approx -3.9 \times 10^4$ dynes/cm². The downstream flow is calculated from the quadratic relation as described previously. We assume a fluid density of 1 g/cm³ and a viscosity of 8 g/(cm sec). The Reynolds number is about 2. The value of viscosity is high and may be the reason for not seeing spontaneous oscillations. While we are restricted, for now, to low values of the Reynolds number, this is not outside the range of actual values. For example, values in dogs range from about 0.001 for capillaries to 1000-4500 for major arteries [3]. Thus our value of 2 is in the range of that of small vessels which have been observed to undergo sausage-string collapse [1, 10]. The high viscosity may also be responsible for the tube being pulled toward the downstream cap. Such a large viscosity was needed for numerical stability.

Recent developments in the immersed boundary methodology have made it possible to raise the Reynolds numbers of computations such as these from the current value of 2 at least to 200 if not higher, see for example [17, 23, 24]. An important future direction will be to apply this improved methodology to the flow in collapsible tubes. But the collapse of tubes at Reynolds number of order 1 is also interesting, and perhaps because it is unfamiliar, contains some surprises, as we shall see.

A real collapsible tube, in the laboratory, does not collapse in an axially symmetric manner [14]. The tube begins to get compressed, taking on an elliptical shape, and eventually developing two distinct channels. Since the tube itself has axisymmetric properties, this represents an instability of the axisymmetric state.

It is not clear a priori whether the axisymmetric state of our model tube will be stable or unstable. This may depend on the specific choice of stiffness parameters for the different types of fibers that comprise the tube. If an instability is present, however, we want to see it. Therefore, we start the tube in a non-axisymmetric configuration. This is done as follows. Once the tube is defined its points are perturbed in one Cartesian direction so that the tube takes on an elliptical shape. The amount of eccentricity varies sinusoidally along the length of the tube, so that both ends remain circular and fixed, and maximum eccentricity occurs at the center of the tube. Figure 1 shows the initial configuration of the perturbed tube (without extensions or caps). For clarity, only a fraction of the helical and longitudinal fibers

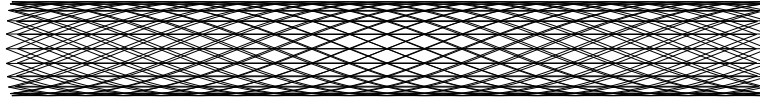


FIGURE 1. Initial configuration of the elastic tube, showing a subset of the helical and longitudinal fibers. The tube is shown in perspective, viewed from a position that lies outside the tube on one of the perpendicular bisectors of the tube axis.

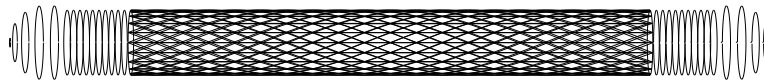


FIGURE 2. Initial configuration of the elastic tube, including rigid extensions and end caps, shown in perspective.

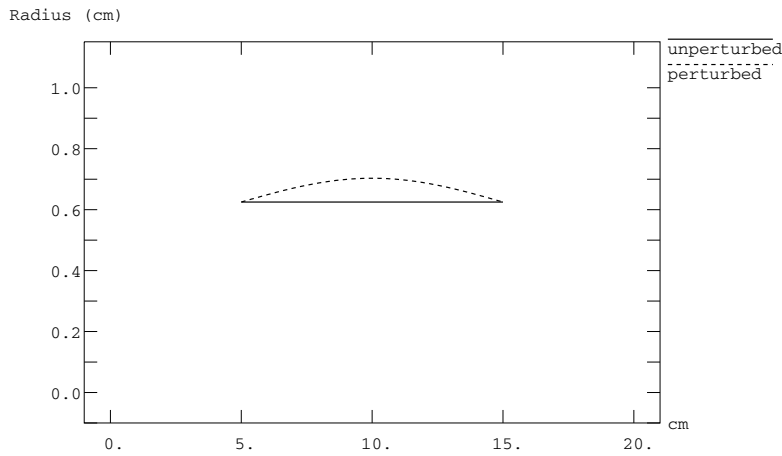


FIGURE 3. Radius (cm) of the tube (of Figure 1) plotted against axial distance (cm) along the tube, in two orthogonal directions. In one direction the tube is unperturbed (lower curve), while it is perturbed in the orthogonal direction (upper curve). The tube, which is taken to be 10 cm long, is centered in the computational lattice, which is 20 cm long.

are shown; the rings are not shown. Figure 2 shows the initial configuration with the extensions and caps.

Figure 3 shows the radial distance from the axis of the perturbed tube along two perpendicular Cartesian directions. Along one direction the tube is unperturbed (lower curve), while it has its maximum perturbation in the orthogonal direction. The amount of perturbation varies smoothly in the intermediate directions. (Note that, although the computational region is 20 cm long, the figure shows only the elastic region of the tube which is 10 cm long, centered in the computational region, from 5 cm to 15 cm. The remaining 10 cm of the computational region contain the

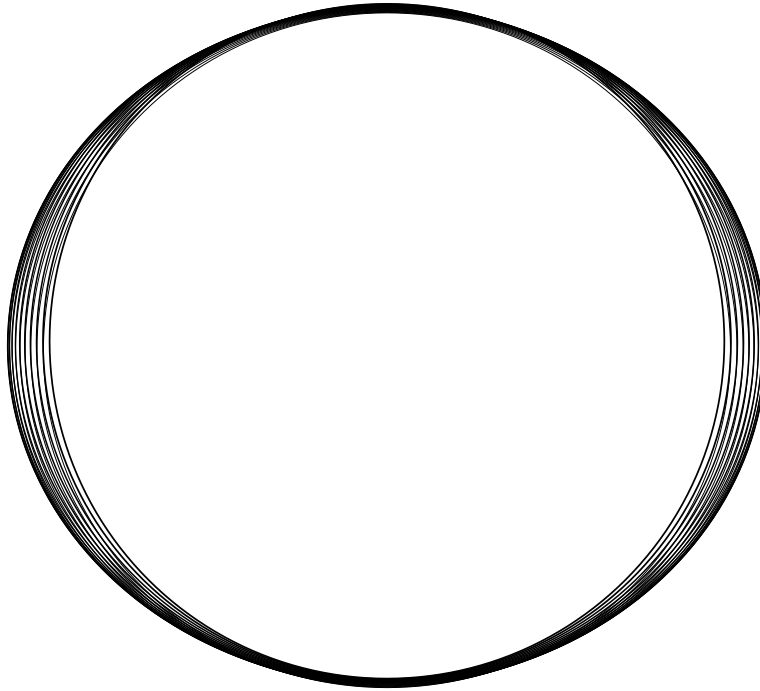


FIGURE 4. Superposition of cross sections, equally spaced along the length of the tube (of Figure 1). The size and direction of the perturbation from cylindrical symmetry are shown.

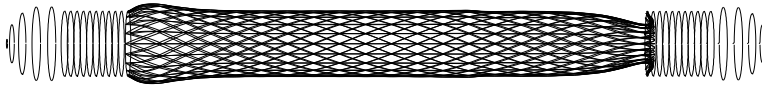


FIGURE 5. Elastic tube with rigid extensions and caps at a later time. The beginning of collapse is visible at the downstream (right) end. In addition an initial bulge is visible at the upstream end.

rigid supports and the end caps which are not shown in the figure.) Figure 4 shows the initial position of the rings in a two dimensional projection plot. It is, in effect, a superposition of successive cross sections taken along the length of the tube. In it we can see the amount of variation in the shape of the cross sections of the tube. In this particular example, the maximum amount of perturbation is 20%.

Figures 5, 6, and 7 show the tube, cross sections and radius at a later time. The cross sections become more nearly circular with time, thus showing that the tube is tending towards axial symmetry. The tube shows an initial bulge in the upstream end and collapse at the downstream end. The downstream end has been pulled into the extension slightly. Thus, with the particular parameters chosen here, the axisymmetric mode of collapse is stable, since the tube tends towards an axisymmetric configuration and we will not observe asymmetric buckling. Although exact

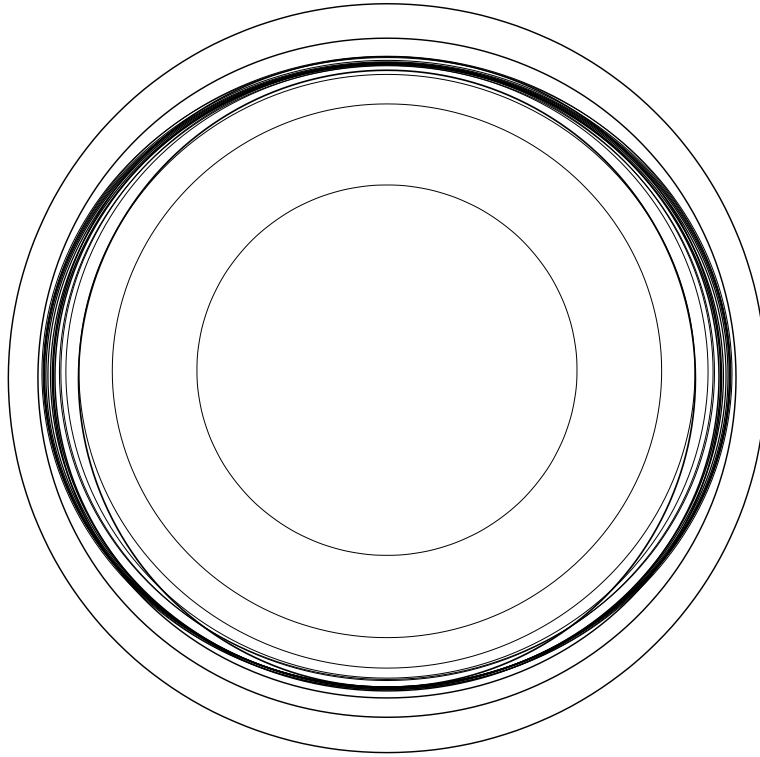


FIGURE 6. Superposition of cross sections, equally spaced along the length of the tube (of Figure 5). While some deviation from axial symmetry is still visible, we can see that the tube is tending toward symmetry, showing that, for the particular set of stiffness parameters, the axisymmetric mode of the collapse is stable.

comparisons are not possible, qualitatively, the behavior of the radius shows similarities with axisymmetric deformations in other studies of pre-buckling behavior in fluid-carrying cylindrical shells [12, 13].

By increasing the stiffness of the hoop fibers, we arrived at the next example. The initial configuration of the tube, together with its extensions and caps, was the same as before. In Figures 8 and 9 we again see the state of the tube and the radius along the length of the tube, at some time during the simulation. In these figures we can clearly see the collapse of the downstream end. The amount by which the tube has been drawn into the rigid extension at the downstream end has been reduced by the inclusion of what we have termed a “screen force” at that end. For each point of the tube, we have added a Hooke’s law type restoring force, proportional to the amount by which the point has passed the clamped end of the tube in the axial direction. (The particulars of this force, including its energy function, etc. are just like that of the spring force associated with the caps, except that here the springs are one-dimensional and one-sided, i.e., they respond only to

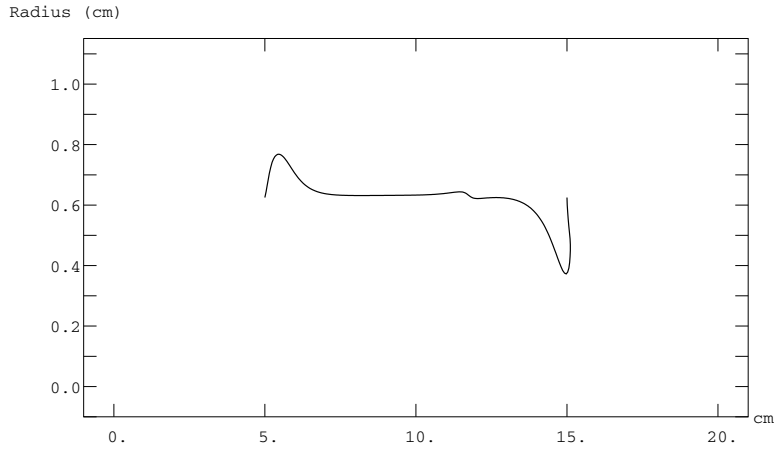


FIGURE 7. Radius (cm) of the tube (of Figure 5) plotted against axial distance (cm) along the tube. Note that the vertical scale has been expanded to show detail. The upstream bulge and downstream collapse are clearly visible. Also note that the downstream end has been pulled passed the clamped end of the tube and into the extension slightly.

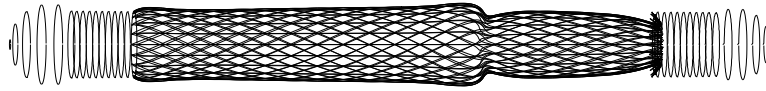


FIGURE 8. Elastic tube with rigid extensions and caps undergoing collapse. The upstream bulge and downstream collapse are seen.

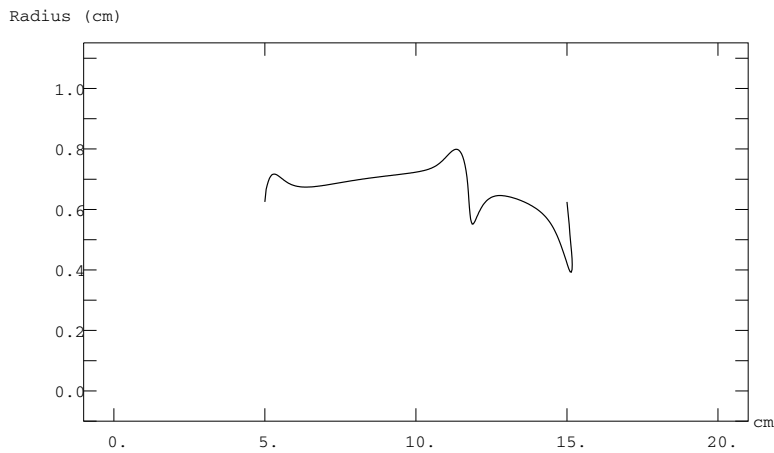


FIGURE 9. Radius (cm) of the tube (of Figure 8) plotted against axial distance (cm) along the tube, with an expanded vertical scale to show detail.

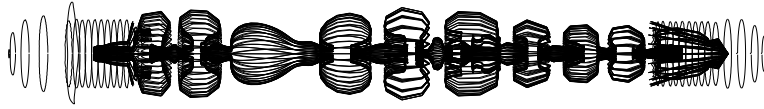


FIGURE 10. An instance of the model where the tube has displayed multiple regions of partial collapse separated by noncollapsed segments of the tube.

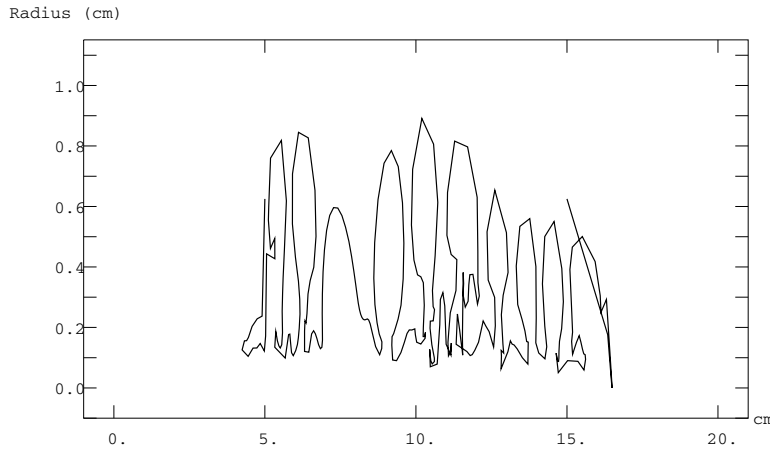


FIGURE 11. Radius (cm) of the tube (of Figure 10) displaying multiple regions of partial collapse, plotted against axial distance (cm) along the tube, with an expanded vertical scale to show detail. Note the partial inversion of the tube where collapse is observed.

the x_1 component of displacement, and then only when that displacement is in the downstream direction.)

By further increasing the bending rigidity of the fibers, we have been able to demonstrate an interesting phenomenon. The tube has developed multiple regions of partial collapse which are separated by non-collapsed segments (Figures 10 and 11). Partial inversion of the tube at each segment of collapse is seen. This inversion seems to be a consequence of the longitudinal bending rigidity, which smooths out the discontinuities that would otherwise occur at the borders between the collapsed and uncollapsed regions. Instead of smoothing in the manner one might expect, in which the radius of the tube would remain a single-valued function of axial position, the tube takes advantage of the opportunity to fold back on itself to reduce the bending energy even further.

Although multiple regions of collapse are not observed in typical laboratory experiments on collapsible tubes, they are seen in *small* blood vessels constricting in response to high blood pressure [1, 11]. We quote the description of this phenomenon from [1]: “As the infusion is continued, a substantial narrowing of the smaller blood vessels is observed, and suddenly the narrowed vessels develop a peculiar pattern consisting of alternating regions of constrictions and dilations, giving the vessels the appearance of sausages on a string... The sausage-string pattern has

been observed in the small vessels of many organs, including the brain, the gut, and the kidney...”

It is paradoxical that these blood vessels are decreasing in radius and eventually collapsing as the blood pressure is increased. Presumably, the reason for this is a muscular reflex which constricts the vessels in response to elevated blood pressure. The constricting force of the muscles is at least qualitatively analogous to an increase in external pressure, and it sets the stage in a similar way for collapsible tube phenomena to occur. That the manner of collapse is similar to that seen in our computational experiments may be coincidental, but it is at least worthy of further investigation.

7. Conclusions and future work

This paper describes a numerical method to simulate the behavior of fluid flow through a collapsible tube. It is unique in that it simulates this behavior of an elastic tube in three spatial dimensions without relying on any simplifications associated with assumed symmetries of the tube. It uses the improved volume conservation version [38] of the immersed boundary method in three dimensions, a version which has previously been implemented only in two dimensions.

The program that implements this numerical method calculates the velocity, pressure, and force fields at each point on a three dimensional lattice, and also the position and shape of the immersed boundary forming the tube, at discrete points in time. Video animations of the data have been made, and thus the “actual” motion of the fluid and tube can be observed.

Results obtained to date have emphasized the transient collapse of an initially open tube. In most cases, (partial) collapse is seen primarily near the downstream end of the tube, but in others, the collapsible tube partitions itself into sections of open tubing separated by sections in which (partial) collapse has occurred.

In future work, we plan to lower the viscosity of the fluid. This will require a modification of the numerical method used for the fluid dynamics. Fortunately, the immersed boundary method is modular in the sense that the Navier-Stokes solver can be changed without requiring changes in the other parts of the code. Lowering the viscosity should make it possible to simulate the spontaneous oscillations that are commonly observed in collapsible tube experiments, and it should also broaden the range of phenomena to which the methodology described here may be applied. It will also allow for more complete comparison with solutions from other methods. Another project for the future is to study the problem of non-axisymmetric vs. axisymmetric collapse, both through stability analysis of the axisymmetric state and through numerical experiments on tubes that collapse in an asymmetric manner. Finally, we plan to apply the methodology described here to biomechanical problems in which collapsible tube phenomena play a significant role, such as the fluid dynamics of veins and pulmonary airways (especially in asthma), and renal tubules.

Acknowledgements. The authors are indebted to David M. McQueen for helpful discussions throughout the research described in this paper.

References

- [1] P. Alstrom, V. M. Eguiluz, M. Colding-Jorgensen, F. Gustafsson, and N. Holstein-Rathlou, *Instability and 'sausage-string' appearance in blood vessels during high blood pressure*, Phys. Rev. Lett. **82** (1999), 1995–1998.
- [2] C. D. Bertram and T. J. Pedley, *A mathematical model of unsteady collapsible tube behavior*, J. Biomechanics **15**, (1982), 39–50.
- [3] C. G. Caro, T. J. Pedley, R. C. Schroter, and W. A. Seed, *The Mechanics of the Circulation*, Oxford University Press, 1978.
- [4] A. J. Chorin, *Numerical solution of the Navier-Stokes equations*, Math Computations **22** (1968) 745–762, MR 39 #3723, Zbl 0198.50103.
- [5] A. J. Chorin, *On the convergence of discrete approximations to the Navier-Stokes equations*, Math Computations **23** (1969), 341–353, MR 39 #3724, Zbl 0184.20103.
- [6] W. A. Conrad, *Pressure-flow relationships in collapsible tubes*, IEEE Transactions on Biomedical Engineering **BME-16** (1969), 284–295.
- [7] W. A. Conrad, D. M. McQueen, and E. L. Yellin, *Steady pressure flow relations in compressed arteries: Possible origin of Korotkoff sounds*, Med. and Biol. Eng. and Comput. **18** (1980), 419–426.
- [8] W. A. Conrad, C. S. Peskin, and D. M. McQueen, *A piecewise linear model of steady flow in a collapsible tube*, EUROMECH Colloquium 137: Flow in Collapsible Tubes, Cambridge, England, January, 1981 (Abstract).
- [9] J. E. Flaherty, J. B. Keller and S. I. Rubinow, *Post buckling behavior of elastic tubes and rings with opposite sides in contact*, SIAM J. Appl. Math. **23** (1972), 446–455, Zbl 0249.73046.
- [10] Y. C. Fung, *Biomechanics Circulation*, 2nd ed, Springer-Verlag, 1984.
- [11] F. Gustafsson, *Blood Pressure* **6** (1997), 71.
- [12] M. Heil, *The stability of cylindrical shells conveying viscous fluid*, J. of Fluids and Structures **10** (1996), 173–196.
- [13] M. Heil and T. J. Pedley, *Large axisymmetric deformation of a cylindrical shell conveying a viscous flow*, J. of Fluids and Structures **9** (1995), 237–256.
- [14] O. E. Jensen and T. J. Pedley, *The existence of steady flow in a collapsed tube*, J. Fluid Mech. **206** (1989), 339–374.
- [15] R. D. Kamm and A. H. Shapiro: *Unsteady flow in a collapsible tube subjected to external pressure or body forces*, J. Fluid Mech. **95** (1979), 1–78.
- [16] I. Kececioglu, M. E. McClurken, R. D. Kamm and A. H. Shapiro, *Steady, supercritical flow in collapsible tubes. Part 1. Experimental observations*, J. Fluid Mech. **109** (1981), 367–389.
- [17] M.-C. Lai and C. S. Peskin, *An immersed boundary method with formal second order accuracy and reduced numerical viscosity*, J. Comput. Phys. **160** (2000), 705–719, MR 2000m:76085.
- [18] R. J. LeVeque and Z. Li, *Immersed interface methods for Stokes flow with elastic boundaries or surface tension*, SIAM J. on Sci. Comp. **18** (1997), 709–735, Zbl 0879.76061.
- [19] M. E. McClurken, I. Kececioglu, R. D. Kamm and A. H. Shapiro *Steady, supercritical flow in collapsible tubes. Part 2. Theoretical studies*, J. Fluid Mech. **109** (1981), 391–415.
- [20] Y. Matsuzaki and T. Matsumoto, *Flow in a two-dimensional collapsible channel with rigid inlet and outlet*, Trans. of the ASME. **111** (1989), 180–184.
- [21] D. M. McQueen, private communication.
- [22] D. M. McQueen and C. S. Peskin, *A Three-Dimensional Computational Method for Blood Flow in the Heart II. Contractile Fibers*, J. Comput. Phys. **82** (1989), 289–297, Zbl 0701.76130.
- [23] D. M. McQueen and C. S. Peskin, *Heart simulation by an Immersed Boundary Method with formal second-order accuracy and reduced numerical viscosity*, Proceedings of the International Conference on Theoretical and Applied Mechanics (ICTAM) 2000, in press.
- [24] D. M. McQueen, C. S. Peskin, and L. Zhu, *The immersed boundary method for incompressible fluid-structure interaction*, Proceedings of the First M.I.T. Conference on Computational Fluid and Solid Mechanics, June 12–14, 2001, in press.
- [25] P. Morgan and K. H. Parker, *A mathematical model of flow through a collapsible tube. I. Model and steady flow results*, J. of Biomech. **22** (1989), 1263–1270.
- [26] T. J. Pedley, *The fluid mechanics of large blood vessels*, Chapter 6, Flow in Collapsible Tubes, Cambridge Univ. Press, Cambridge, 1980.

- [27] T. J. Pedley, *Wave phenomena in physiological flows*, IMA J. of App. Math. **32** (1984), 267–287, MR 85b:76076.
- [28] C. S. Peskin: *Flow Patterns Around Heart Valves: A Digital Computer Method for Solving the Equations of Motion*. Ph.D. thesis, Physiology, Albert Einstein College of Medicine. University Microfilms #72-30, 1972.
- [29] C. S. Peskin, *Numerical analysis of blood flow in the heart*, J. Comput. Phys. **25** (1977), 220-252, MR 58 #9389.
- [30] C. S. Peskin and D. M. McQueen, *Modeling prosthetic heart valves for numerical analysis of blood flow in the heart*, J. Comput. Phys. **37** (1980), 113–132, MR 81g:92011, Zbl 0447.92009.
- [31] C. S. Peskin and D. M. McQueen, *A three-dimensional computational method for blood flow in the heart. I. Immersed elastic fibers in a viscous incompressible fluid*, J. Comput. Phys. **81**, (1989), 372–405, MR 90k:92018, Zbl 0668.76159.
- [32] C. S. Peskin and D. M. McQueen, *A general method for the computer simulation of biological systems interacting with fluids*, Biological Fluid Dynamics (C. P. Ellington and T. J. Pedley, editors), The Company of Biologists Limited, Cambridge UK, 1995, pp. 265–276.
- [33] C. S. Peskin and D. M. McQueen, *Fluid dynamics of the heart and its valves*, Case Studies in Mathematical Modeling: Ecology, Physiology, and Cell Biology (H. G. Othmer, F. R. Adler, M. A. Lewis, and J. C. Dallon, editors), Prentice-Hall, Upper Saddle River NJ, 1996, pp. 309–337.
- [34] C. S. Peskin, D. M. McQueen, and S. Greenberg, *Three-dimensional fluid dynamics in a two-dimensional amount of central memory*, Wave Motion: Theory, Modeling, and Computation, Math. Sci. Res. Inst. Publ., no. 7, Springer, New York, 1987, pp. 85–146, MR 89a:76002, Zbl 0644.76028.
- [35] C. S. Peskin, B. F. Printz, *Improved volume conservation in the computation of flows with immersed elastic boundaries*, J. Comput. Phys. **105** (1993), 33–46, MR 93k:76081, Zbl 0762.92011.
- [36] J. A. G. Rhodin, *Architecture of the vessel wall*, Handbook of Physiology, Section 2: The Cardiovascular System. Am. Physiological Society, 1980.
- [37] M. E. Rosar: *A Three-Dimensional Computer Model for Fluid Flow Through a Collapsible Tube*. Ph. D. thesis, New York University. University Microfilms #9514416 (1994).
- [38] M. E. Rosar, and C. S. Peskin: *Improved Volume Conservation in Three Dimensional Computations of Flows with Immersed Elastic Boundaries*, William Paterson Univ., Technical Report No. 128, 2000.
- [39] C. C. Vesier and A. P. Yoganathan, *A computer method for simulation of cardiovascular flow fields: Validation of approach*, J. Comput. Phys. **99** (1992), 271–287, Zbl 0741.92007.
- [40] J. Womersley, WADC Report TR56-614, 1957 (unpublished).
- [41] J. Womersley, *Flow in the larger arteries and its relation to the oscillating pressure*, J. Physiol. **124** (1954), 31–32P.
- [42] J. Womersley, *Oscillatory motion of a viscous liquid in a thin-walled elastic tube. I. The linear approximation for long waves*, Phil. Mag., **46** (1955), 199–221.

DEPARTMENT OF MATHEMATICS, WILLIAM PATERSON UNIVERSITY, WAYNE, NEW JERSEY 07470
 rosarm@wpunj.edu <http://euphrates.wpunj.edu/faculty/rosarm/>

COURANT INSTITUTE OF MATHEMATICAL SCIENCES, NEW YORK UNIVERSITY, NEW YORK, NEW YORK 10012

peskin@cims.nyu.edu <http://www.math.nyu.edu/faculty/peskin/>

This paper is available via <http://nyjm.albany.edu:8000/j/2001/7-18.html>.